Available online at www.sciencedirect.com

ScienceDirect

Geochimica et Cosmochimica Acta 212 (2017) 221–233

Geochimica et Cosmochimica Acta

www.elsevier.com/locate/gca

Dynamics of ferrihydrite-bound organic carbon during microbial Fe reduction

Dinesh Adhikari [a], Qian Zhao [a], Kamol Das [a], Jacqueline Mejia [b], Rixiang Huang [c], Xilong Wang [d], Simon R. Poulson [e], Yuanzhi Tang [c], Eric E. Roden [f], Yu Yang [a,*]

[a] *Department of Civil and Environmental Engineering, University of Nevada-Reno, MS258, 1664 N. Virginia Street, Reno, NV 89557, USA*
[b] *Environmental Chemistry and Technology Program, Department of Civil and Environmental Engineering, The University of Wisconsin-Madison, 660 North Park Street, Madison, WI 53706, USA*
[c] *School of Earth and Atmospheric Sciences, Georgia Institute of Technology, 311 Ferst Drive, Atlanta, GA 30332-0340, USA*
[d] *Laboratory for Earth Surface Processes, College of Urban and Environmental Sciences, Peking University, Beijing 100871, China*
[e] *Department of Geological Sciences & Engineering, University of Nevada-Reno, MS172, 1664 N. Virginia Street, Reno, NV 89557, USA*
[f] *Department of Geoscience, University of Wisconsin-Madison, 1215 West Dayton St., Madison, WI 53706, USA*

Received 27 January 2017; accepted in revised form 12 June 2017; Available online 17 June 2017

Abstract

The dynamics of iron (Fe)-bound organic carbon (OC) during dissimilatory microbial Fe(III) reduction has the potential to play an important role in regulating the biogeochemical cycling of carbon (C) in permanently or transiently anoxic soils and sediments. In this study, we investigated the release and transformation of ferrihydrite (Fh)-bound OC during microbial reduction of Fe by *Shewanella putrefaciens* strain CN32 under a fixed Fe concentration of 13 mM and varying C/Fe molar ratios. We found that reduction of Fe and reductive release of OC was dependent on the C/Fe molar ratio, with high C/Fe ratio enhancing both reduction of Fe and release of OC. For Fh-OC co-precipitates with C/Fe ratio of 3.7, 54.7% of Fh-bound OC was released to solution phase when 25.1% of Fe was reduced. The presence of OC inhibited the transformation of Fh to more crystalline Fe phases both in the bulk and on the surface. Upon reduction, Fh-bound OC became more concentrated on the surface of Fh-OC co-precipitates, and surface components were enriched with carboxylic functional groups. Reduction increased the lability of Fh-bound OC for Fh-OC co-precipitate with C/Fe ratio of 3.7, and aromatic OC was preferentially retained within the co-precipitates. Our results indicate that microbial reduction altered the quantity and composition of OC released from Fh-OC co-precipitates, depending on the C/Fe ratio and associations between Fe and OC. Assuming higher availability of released OC compared to original Fh-bound OC, reduction of Fh can likely lead to enhanced degradation of OC and result in a shorter residence time for OC in soils and sediments.

Keywords: Ferrihydrite; Organic carbon; Microbial reduction; Degradation and mineralization; Mineral phase transformation

1. INTRODUCTION

Ferrihydrite (Fh), a poorly crystalline iron (Fe) oxide, is an important Fe oxide mineral phase in soils, especially Spodosols and soils with relatively high organic matter content (Cornell and Schwertmann, 1996; Jambor and Dutrizac, 1998). Fh can potentially play an important role in regulating the biogeochemical cycling of carbon (C). Iron oxide minerals have been demonstrated to bind a substantial amount of organic carbon (OC) in soils and sediments globally (Wagai and Mayer, 2007; Lalonde et al., 2012; Zhao et al., 2016). Fh has a higher capacity to bind OC

* Corresponding author.
E-mail address: yuy@unr.edu (Y. Yang).

http://dx.doi.org/10.1016/j.gca.2017.06.017
0016-7037/

compared to other highly crystalline Fe oxides minerals because of its higher surface area and incorporation of OC during precipitation, with the ratio of C/Fe as high as 17.5 for Fh-OC co-precipitates (Tipping, 1981; Gu et al., 1995; Kaiser and Guggenberger, 2007; Chen et al., 2014). Understanding the dynamics of Fh-bound OC is, therefore, critical for evaluating and predicting the turnover of OC in natural soil and sedimentary environments.

Fh can be reduced by abiotic agents as well as dissimilatory metal-reducing bacteria (DMRB) in natural soils and sediments (Roden, 2003, 2006; Weber et al., 2006). Because of the high surface area of Fh, its reduction is relatively faster compared to more crystalline Fe oxides (Bose et al., 2009; Shimizu et al., 2013). The reduction can also lead to mineral phase transformations of Fh, generating secondary minerals such as magnetite, goethite, lepidocrocite, siderite, and akaganeite (Hansel et al., 2003; Kukkadapu et al., 2003). The mineral phase transformation of Fh during the microbial reduction can potentially weaken or break down the associations between Fh and OC and release Fh-bound OC, which has been rarely studied (Elsner et al., 2004). In addition, the transformation of OC during reductive reaction can significantly affect its consequent fate, including degradation and mineralization (Adhikari and Yang, 2015; Adhikari et al., 2016). Previous studies have also demonstrated that OC can be actively involved in Fe reduction as an electron shuttle (Chacon et al., 2006; Zhao et al., 2017). Such involvement of OC in Fe reduction can likely enhance the release and transformation of Fe-bound OC. Therefore, uncovering how Fh-bound OC is released and transformed upon reduction is important for understanding the fate of Fe-bound OC in natural soils.

In this study, we investigated the release and transformation of OC in Fh-OC co-precipitates during reduction by *Shewanella putrefaciens* strain CN32 (referred to hereafter as "strain CN32"). Strain CN32 has been used extensively in previous studies of Fe(III) oxide reduction kinetics and Fe mineral phase transformation (Fredrickson et al., 1998; Roden, 2003, 2004; Zhao et al., 2017). Synthetic Fh-OC co-precipitates with a range of C/Fe ratios (0.7–3.7) were prepared to represent Fh-OC co-precipitates in natural soils. The goals of the study were: to (1) analyze the kinetics of Fe reduction and release of Fe-bound OC to the solution phase; (2) characterize Fe mineral phase transformation; and (3) determine how Fh-bound OC is transformed during microbial reduction.

2. MATERIALS AND EXPERIMENTAL SETUP

2.1. Materials and preparation of HA solution

Elliot humic acid (HA) standard, purchased from International Humic Substance Society (IHSS) (Atlanta, GA), was used for the co-precipitate synthesis, as a model OC to represent a variety of organic domains existing in natural OC and study the impact of co-precipitated OC on the Fe reduction and OC transformation. The HA contains 59.5% C, among which 1% as carbonyl, 11% as carboxyl, 41% as aromatic, 6% as acetal, 14% as heteroaliphatic, and 27% as aliphatic domains (Supplementary Data, Table S1, IHSS). All other chemicals used were above analytical grade. Following previous studies (Yang et al., 2011, 2012), HA solutions were prepared by dissolving a predetermined amount of HA in 0.1 mL of 3 M NaOH solution. The mixture was sonicated for 1 h and then diluted to 5 mL with deionized water. Diluted solutions were shaken overnight at 100 rpm at room temperature. The solutions were then centrifuged at 3000 rpm for 20 min, and supernatants were used as HA stock solutions. OC concentrations of HA solutions were measured with a Shimadzu TOC-VCSH (Kyoto, KYT, Japan). The solutions were stored at 4 °C and were used within a week after preparation.

2.2. Bacteria incubation

Pure cultures of strain CN32 were maintained under aerobic conditions on Luria Broth (LB) agar at 4 °C. Cells were aseptically transferred to 25 g/L LB medium and incubated at 30 °C for 14–16 h to achieve the stationary phase. Cells were centrifuged at 10,000 rpm for 5 min, and the remaining media were decanted. The cell pellets were then washed three times with deoxygenated 3 mM sodium bicarbonate (pH adjusted to 7 ± 0.2 using 0.1 M HCl) buffer by adding 40 mL of fresh buffer, vortexing the mixture, and then centrifuging the suspension at 10,000 rpm for 5 min.

2.3. Fh and Fh-OC co-precipitate synthesis

Fh was synthesized by neutralizing a 0.01 M $FeCl_3$ solution from its original pH of around 1.8 to pH 7.5 with 0.04 M NaOH following previous studies (Hansel et al., 2004; Shimizu et al., 2013). Once the desired pH was achieved, the precipitated oxides were allowed to settle for around 15 min, and the supernatant was decanted. The process of settling the co-precipitates and decanting the supernatant was repeated 3 times. Then the precipitate was centrifuged at 7000 rpm for 10 min, and the supernatant was discarded. After 3 deionized water rinses, the precipitate was left in the slurry and stored at 4 °C for future use. Fresh synthesized Fh was used within 2 months after synthesis. For synthesizing Fh-OC co-precipitates, pre-determined amounts of HA solution were added to 0.01 M $FeCl_3$ solution, and the mixtures were neutralized to pH 7.5 using 0.04 M NaOH. The molar ratios of C/Fe in feedstock solutions were set at 0.5, 1, 2, and 4. The co-precipitates were rinsed and stored, following the same protocol for Fh. Iron concentration in the co-precipitates was determined by dissolving the co-precipitates in 12 M HCl, reducing Fe(III) with hydroxylamine hydrochloride (10% w/v hydroxylamine hydrochloride in 1 M HCl), and analyzing Fe(II) concentration using the ferrozine assay (1% w/v ferrozine in 50% w/v ammonium acetate (Stookey, 1970; Hansel et al., 2003; Xu et al., 2016). Carbon content in co-precipitates was measured using an elemental analyzer (EuroVector SpA, Milan, Italy). Based on the measurement, the actual molar ratios of C/Fe for the synthesized co-precipitates were 0.7 ± 0.06, 0.9 ± 0.02, 1.8 ± 0.05 and 3.7 ± 0.45. The recoveries for Fe and OC in the co-precipitates were $86.3 \pm 12.7\%$ and $94.0 \pm 4.7\%$. The parti-

cle size of Fh and Fh-OC co-precipitates was measured using a Dynamic Light Scattering Analyzer (Nicomp Particle Sizing System, Santa Barbara, CA, USA). In addition, the surface area of Fh and Fh-OC co-precipitates was estimated based on the empirical model fitting for the relationship between surface area and C/Fe ratio using the data from Shimizu et al. (2013) (Supplementary Data, Fig. S1). The basic characterizations for the Fh and Fh-OC co-precipitates have been summarized in Table S2 (Supplementary Data).

2.4. Reduction of Fe and reductive release of Fe-bound C

Fh and Fh-OC reduction experiments were conducted under anaerobic atmosphere in a Coy glove box (6% H_2, 94% N_2). The H_2 in the headspace served as an electron donor for microbial reduction (Chacon et al., 2006). To minimize the ramification in quantifying the release of Fh-bound OC, no additional OC as a carbon source or electron donor was added. The buffer solution consisted of 3 mM $NaHCO_3$ (pH = 7), which was purged with N_2 gas for 1 hour to remove dissolved oxygen. An aliquot of co-precipitate was mixed with strain CN32 in the buffer, with the final bacterial concentration of 10^8 cell/mL and final sample volume of 5 mL in 20 mL glass amber vials. Initial Fe concentration was set at 13 mM. The vials were sealed with air-tight caps, and the samples were shaken at 150 rpm at 25 °C. At certain time points within a 288 h period, triplicate samples were sacrificed for analysis of Fe(II) and OC release. Through the experiment, the pH of the system remained stable around 7.2 ± 0.2. The system of pure (OC-free) Fh with strain CN32 was used as the biotic control. For Fh-OC with C/Fe ratio of 0.7 and 3.7, we conducted abiotic controls by mixing Fh-OC with the buffer solution only.

For the solution phase Fe(II) analysis, 1 mL of sample was centrifuged and the supernatant was analyzed for Fe (II) using ferrozine assay (1% w/v ferrozine in 50 mM PIPES at pH7) (Xu et al., 2016). To determine total Fe (II) (solution phase + solid-associated) concentration, 175 μL of 12 M HCl was added to the remaining 4 mL of slurry (final HCl concentration of 0.5 M), and the mixture was analyzed for Fe(II) after 24 h using the ferrozine assay (Eusterhues et al., 2014a,b; Xu et al., 2016). The concentration of solid-associated Fe(II) was determined as the difference between the total and solution phase Fe(II). For OC in the solution phase, the samples were centrifuged at 12,000 rpm for 10 min, and the supernatants were analyzed using a Shimadzu total organic carbon analyzer (TOC)-VCSH (Kyoto, KYT, Japan).

2.5. Desorption experiment

We analyzed desorption kinetics of the Fe-bound OC before and after the reduction under oxic condition as an indicator for its lability. An aliquot of co-precipitate was mixed with deionized water to achieve Fe concentration of 13 mM, and the samples were then shaken at 200 rpm. At different time points within 96 h, the samples were centrifuged at 12,000 rpm for 10 min and the supernatant was analyzed for dissolved OC (DOC) concentration (mg C/L) using a Shimadzu TOC-VCSH (Kyoto, KYT, Japan).

3. ANALYTICAL TECHNIQUES

3.1. X-ray diffraction (XRD) analysis

The Fh and Fh-OC co-precipitates were analyzed using a powder XRD diffractometer (Philips Electronic Instruments, Mahwah, NJ, USA). XRD was analyzed for the 2θ range of 20–90°, with a step size of 0.02°. Data was analyzed using the software JADE (Jacksonville, FL, USA).

3.2. X-ray absorbance spectroscopy (XAS) analysis

Iron K-edge XAS spectra were collected at beamline 4-1 of Stanford Synchrotron Radiation Lightsource using a 13-element Ge detector. Energy calibration used a Fe foil. A thin layer of sample slurries was dried on Kapton tape in a Coy glove box (95% N_2, 5% H_2) at the beamline, immediately sealed with Kapton tape, transferred to a sample chamber cooled with liquid nitrogen, and purged by He gas to prevent potential beam-induced oxidation. Both fluorescence and transmission data were collected and compared. Multiple scans were collected for each sample and averaged. Data analysis was conducted using the programs Sixpack and Ifeffit (Newville, 2001; Webb, 2005). Principle component analysis (PCA) was conducted on the data to evaluate the number of end member components needed for reconstructing the data. Identification and quantification of the unknown Fe mineral phases were determined by linear combination fitting (LCF) for the k^3-weighted EXAFS of the unknown sample spectra using a library of Fe reference compounds, including siderite, 2-line ferrihydrite, goethite, lepidocrocite, hematite, green rust, akaganeite, magnetite, and an Fe(III)-organic matter [Fe(III)-OM] co-precipitate (formed by precipitating $Fe(NO_3)_3$ with dissolved organic matter extracted from field-fresh samples of a forest floor layer at pH ~ 2.6) (Chen et al., 2014). LCF of the empirical model spectra were optimized where the only adjustable parameters were the percent of each model compound contributing to the fit. The goodness of fit was established by minimization of the R-factor (Newville, 2001).

3.3. Near edge X-ray absorbance fine structure (NEXAFS) analysis

Carbon 1 s NEXAFS analysis was performed for co-precipitates with C/Fe ratio of 0.7 and 3.7 (before and after reduction) on the X-ray absorption spectroscopy endstation on the SGM beamline at Canadian Light Source (Saskatoon, Canada) (Lehmann et al., 2009). An aliquot of sample was loaded onto a gold-coated silicon wafer attached to a copper holder for the analysis. The beamline has an energy range of 250–2000 eV, spot size of 1000 μm × 100 μm, and a 45-mm planer undulator. A silicon drift detector (SSD) and titanium filter were used for the data collection. Scans were acquired from 270 to 320 eV with 0.2 eV step size.

3.4. X-ray photoelectron spectroscopy (XPS)

XPS was used to analyze the surface chemical compositions and speciation of Fh and Fh-OC co-precipitates. Elemental survey scan, Fe2p, and C1s scan were obtained using an AXIS-Ultra instrument (Kratos Analytical, Manchester, United Kingdom) with monochromatic Al Kα radiation (225 W, 15 mA, 15 kV). Quantification of Fe phases on the surface was determined by the deconvolution of XPS spectra using a library of XPS for Fe compounds in the co-precipitates (identified by EXAFS analysis). For C1s spectra, we calibrated binding energies using C1s peak at 284.8 eV. Data analysis was performed using CasaXPS software package. C1s binding energies were assigned as: C—C (284.6 eV), C—O—C (286.2 eV), C═O (287.6 eV) and COOH (289.1 eV) (Cheng et al., 2006; Nguyen et al., 2008).

3.5. Specific ultraviolet absorbance (SUVA) analysis

SUVA at 254 nm ($SUVA_{254}$) was analyzed for the OC released to the solution phase, as an index for aromaticity (Weishaar et al., 2003). To minimize the influences of Fe (II) and dissolved biomolecules, the released OC was recovered through a previously developed precipitation-re-dissolution method, because the model OC (humic acid) could precipitate out at low pH (Adhikari and Yang, 2015). The samples after reduction were centrifuged at 12,000 rpm for 10 min, and supernatants were collected. For precipitation of released OC, the pH value of supernatants was lowered to below 2 by adding concentrated HCl. After precipitation, the samples were centrifuged at 12,000 rpm for 10 min, and the supernatants were decanted. The precipitates were dissolved in 1 M NaOH. Based on our test, $106 \pm 13\%$ of HA was recovered through this precipitation-re-dissolution process. Using the same protocol, we also determined that the recovery of OC mixed with bacteria (CN32) was $104 \pm 2\%$. For the solutions with re-dissolved OC, UV absorbance at 254 nm was measured using Evolution 260 BIO (Thermo Scientific, Waltham, MA) in a 10 mm quartz cuvette. $SUVA_{254}$ was calculated using:

$$SUVA_{254} = \frac{UV_{254}}{TOC \cdot L} \quad (1)$$

where $SUVA_{254}$ is the specific UV absorbance at 254 nm (L mg C^{-1} m^{-1}), UV_{254} is the UV absorbance at 254 nm, TOC is the total organic carbon concentration (mg C/L), and L is the path length (m).

3.6. Thermal gravimetric analysis (TGA)

TGA analysis was performed under N_2 purge (20 mL/min) from 30 to 900 °C with temperature increments of 10 °C/min using a Perkin Elmer STA 6000. The data was analyzed using Pyris software version 9.0.1.0174.

3.7. Statistical analysis and model fitting

T-test and Pearson correlation analysis were performed with IBM SPSS Statistics 24. First order kinetic fitting and other empirical model fittings were conducted with Matlab 2013. Linear regression was done in Microsoft Excel 2016.

4. RESULTS

4.1. Reductive release of Fh-bound OC

A total of 12.5% of Fe in the pure Fh was reduced within 288 h (Fig. 1, Supplementary Data, Fig. S2 and S3). The Fh-OC co-precipitate with a C/Fe ratio of 3.7 was reduced more extensively (25.1%) than the pure Fh, whereas the Fh-OC co-precipitates with lower C/Fe ratios were reduced less than pure Fh. Based on the linear regression for Fe(II) concentration or fraction versus time, Fe in Fh-OC co-precipitate was reduced at a rate of 2.7×10^{-3} to 9.7×10^{-3} mM Fe(II)/h or 2.0×10^{-2} to 7.2×10^{-2}%/h (Supplementary Data, Table S3). The reduction of Fe can also be fitted well with the first order kinetics ($R^2 > 0.90$ for co-precipitates and $R^2 = 0.76$ for ferrihydrite), and the rate constant ranged from 2.05×10^{-4} to 8.24×10^{-4} h^{-1} (Supplementary Data, Figs. S4 and S5, Table S4). Consistently with the results for the reduction rate calculation, the reduction rate constant for pristine Fh was higher than that for co-precipitates with C/Fe ratio of 0.7, 0.9, and 1.8, but lower than that for co-precipitates with C/Fe of 3.7. The surface area-normalized Fe reduction was highest for Fh-OC with C/Fe of 3.7, with 2.21×10^{-3} mmole Fe(II)/m^2 after 288 h reduction (Supplementary Data, Fig. S6 and Table S5).

The release of Fh-bound OC was also dependent on the C/Fe ratio of the co-precipitates. As shown in the bacteria control containing only strain CN32 cells, the release of microbial biomass or extracellular biomolecules contributed 5.3 ± 0.5 to 10.8 ± 2.9 mM C (Supplementary Data, Fig. S7). Use of pure strain CN32 as a control was validated by multiple additional experiments (Supplementary Data, Figs. S8 and S9). Subtracting the bacterial contribution, less than 4.9% of Fe-bound OC in co-precipitates with C/Fe ratio ranging 0.7–1.8 was released during microbial reduction, lower than the percent of Fe reduction. However, for co-precipitates with a C/Fe ratio of 3.7, 54.7% of Fh-bound OC was released at the 288-h reduction period, when 25.1% of Fe was reduced. Bacteria-free controls for Fh-OC co-precipitate with C/Fe ratio of 3.7 showed only minimal (6.3% of total) release of Fe-bound OC, indicating that the abiotic release of Fe-bound OC was much lower than that driven by microbial reduction for co-precipitates with C/Fe of 3.7 (Supplementary Data, Fig. S7).

4.2. Transformation of Fe mineral phase upon reduction

The original Fh and Fh-OC mineral phases were confirmed to be 2-line Fh by XRD analysis (Supplementary Data, Fig. S10). EXAFS analysis with linear combination fitting using multiple reference compounds demonstrated the formation of secondary minerals during reduction (Fig. 2; Supplementary Data, Figs. S11 and S12; Table S6). The co-precipitate C/Fe ratio had a significant

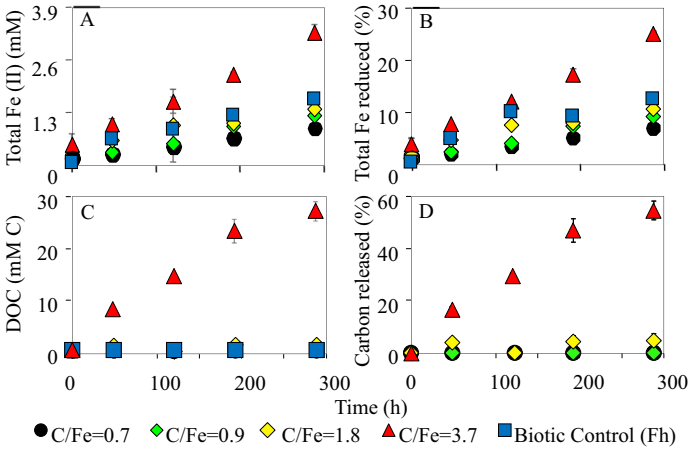

Fig. 1. Fe(II) and dissolved organic carbon (DOC) release for ferrihydrite (Fh)-OC co-precipitates with C/Fe ratios ranging 0.7–3.7: total Fe (II) (solution phase + solid-associated Fe(II)) concentration (A), percentage of total Fe(II) to total Fe (B), DOC concentration (mM C) and percentage of DOC to total OC (TOC) (D). Pure Fh incubated with *Shewanella putrefaciens* CN32 (strain CN32) was used as the biotic control. The DOC was calibrated by subtracting the corresponding data for the bacteria control of only strain CN32 (Supplementary Data, Fig. S2). Error bars indicate standard deviations ($n = 3$), and some are smaller than the symbols.

impact on secondary Fe mineral formation. After 288 h of reduction, pure Fh was completely transformed to goethite (29.0%) and magnetite (71.0%). The percent of secondary minerals decreased with increasing co-precipitate C/Fe ratio. For co-precipitates with C/Fe ratio of 0.7, 0.9 and 1.8, 25.2%, 23.7%, and 44.0% of the Fh were preserved after 288-h of reduction, respectively (Fig. 2; Supplementary Data, Fig. S12; Table S6). For co-precipitate with C/Fe ratio of 3.7, 78.5% of the Fh was preserved (Fig. 2; Supplementary Data, Table S6).

It is more challenging to unambiguously determine the composition of secondary minerals on the surface of the Fh-OC co-precipitates, because of the significant overlap in XPS signals for different Fe mineral phases (McIntyre and Zetaruk, 1977; Grosvenor et al., 2004; Biesinger et al., 2011). Deconvolution of XPS data showed that the generations of secondary mineral phases were similar on the surface compared to the bulk obtained from XAS data (Fig. 3; Supplementary Data, Figs. S13–S14; Table S7). For instance, the Fh-OC co-precipitates with C/Fe ratio of 3.7 had 78.5% of residual Fe as Fh in the bulk, while 75.7% of Fe on the surface stayed as Fh after the reduction. For Fh-OC co-precipitates with C/Fe ratio of 0.7, Fh, lepidocrocite, and akaganéite contributed to 25.2%, 34.7%, and 40.0%, in the bulk, and 23.8%, 35.8%, and 40.4% on the surface, respectively.

4.3. Fate of Fh-bound OC during reduction

4.3.1. Fe-bound OC release

Release of Fh-bound OC during reduction was also dependent on the chemical composition of OC. The presence of Fe prevented the direct analysis of OC chemical composition using nuclear magnetic resonance (NMR) spectroscopy. Instead, we measured $SUVA_{254}$ as an index for the aromaticity of released OC. $SUVA_{254}$ of the released OC increased with increasing C/Fe ratio for the co-precipitates (Fig. 4; Supplementary Data, Table S8). After 288 h reduction, $SUVA_{254}$ values were 1.0 ± 0.8, 0.9 ± 0.5, 4.2 ± 0.2, and 7.4 ± 2.8 L mg C^{-1} m^{-1} for OC released from co-precipitates with C/Fe ratio of 0.7, 0.9, 1.8, and 3.7, respectively. The biotic control experiment (using strain CN32 only) showed very low $SUVA_{254}$ values (0.2 ± 0.04 L mg C^{-1} m^{-1}), indicating that the aromatic carbon input from biomass was negligible.

4.3.2. Fh-OC co-precipitates surface composition

XPS analysis also provided insights into the alteration of OC chemical compositions and Fh-OC associations during the reduction process (Fig. 5; Supplementary Data, Fig. S15 and Table S9). The surfaces of Fh-OC co-precipitates were mainly composed of C, O, and Fe (Fig. 5). C was enriched on the surface (C/Fe ratio = 2.6–15.4), as compared to the bulk (C/Fe ratio = 0.7–3.7) (Supplementary Data, Fig. S16). With increasing bulk C/Fe ratio, the surface C/Fe ratio also increased. More surface-enriched OC prevented Fh from undergoing mineral phase transformation, as demonstrated by EXAFS and XPS analysis of Fe mineral species (Fig. 2; Supplementary Data, Figs. S12 and S13). After 288 h reduction, the surface C/Fe ratio increased significantly from 7.2 to 68 and from 16.0 to 70.3 for co-precipitates with bulk C/Fe ratio of 1.8 and 3.7 respectively (Supplementary Data, Fig. S16).

In addition to the surface enrichment of C, C1s XPS spectra showed a change in the chemical composition of OC on the surface (Fig. 6; Supplementary Data, Fig. S17). Based on the spectra and deconvolution results, the surfaces of original Fh-OC co-precipitates were mainly composed of C—C, C—O—C and COOH, with minor contribution from C=O. The deconvoluted fraction of C—C, C—O—C, and COOH for original Fh-OC co-precipitates ranged 38.5–49.4, 31.1–45.3, and 12.5–18.4%, respectively (Supplementary Data, Table S10). After reduction, the components of C—C increased to 49.6–68.5%, which is

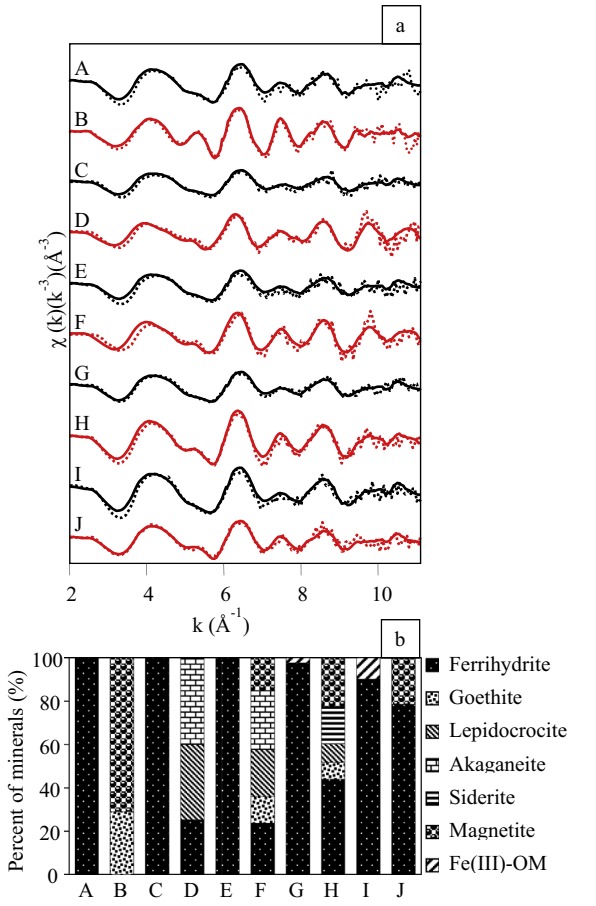

Fig. 2. Fe K-edge extended X-ray absorption fine structure (EXAFS) spectra (a) and fraction of different mineral phases (b) for Fh-OC co-precipitates before and after reduction. Dotted lines represent the original spectra, and the solid lines represent the linear combination fit. A and B represent pure Fh before and after 288-h reduction. C, E, G, and I stand for the original Fh-OC co-precipitates with OC/Fe ratios of 0.7, 0.9, 1.8, and 3.7, respectively. D, F, H and J represent the corresponding Fh-OC co-precipitates after 288-h reduction.

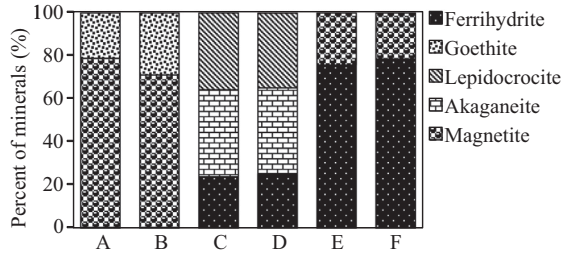

Fig. 3. Comparison of Fe mineral species in the bulk and on the surface of Fh and Fh-OC co-precipitates after 288-h reduction. A, C and E represent the bulk mineral compositions for Fh, Fh-OC with C/Fe ratio of 0.7, and 3.7, respectively. B, D and F represent the surface mineral compositions for Fh, Fh-OC with C/Fe ratio of 0.7 and 3.7, respectively.

mainly contributed by the biomass and biomolecules of strain CN32. C—C usually comprises 50% or more of the cell carbon (Dufrene et al., 1997; Ojeda et al., 2008). XPS

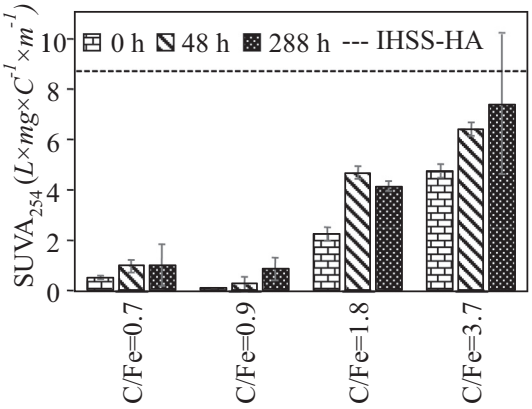

Fig. 4. Specific UV absorbance at 254 nm (SUVA$_{254}$) for the released OC during the microbial reduction of Fh-OC co-precipitates with C/Fe ratio of 0.7, 0.9, 1.8 and 3.7. The released OC was recovered by the precipitation-re-dissolution method. Dashed line represents the value for original IHSS HA.

analysis for a related *Shewanella* species (*S. oneidensis*) showed that its surface carbon was mainly composed of C—C functional groups (Neal et al., 2002). For the biotic control using pure Fh, there was also significant increase in C—C from 36.9% to 50.6%. In parallel, the relative contribution of COOH increased for Fh-OC co-precipitates after the reduction. Ratio of COOH/C—O—C increased from 0.59 to 0.61, 0.31 to 0.49, 0.37 to 0.50, and 0.41 to 1.41 for Fh-OC co-precipitates with C/Fe ratio of 0.7, 0.9, 1.8 and 3.7, respectively. Possible C input from the bicarbonate was ignored as bicarbonate sorption by Fh was minimal, about 0.3 μM-C/m^2-Fh (Zachara et al., 1987; Appelo et al., 2002). Total OC content for C/Fe ratio of 0.7 is about 53 μM/m^2 Fh. Hence, any influence on surface carbon concentration due to bicarbonate sorption would be a small fraction of total OC.

4.3.3. Change in thermal stability

Thermal properties can serve as another indicator for the structure of Fh-OC co-precipitates and the interactions between OC and Fe (Fig. 7; Supplementary Data, Fig. S18). For the original Fh-OC co-precipitates with C/Fe ratio of 0.7 and 0.9, substantial mass loss started at 180 °C, with 68.9% and 61.5% residual mass upon heating to 900 °C. For Fh-OC co-precipitates with higher C/Fe ratios (1.8 and 3.7), the mass loss started at lower temperatures and at a higher rate, which was partially contributed by the lower mass fraction of Fe oxides. To account for the influences of residual Fe oxides, we calculated the residual fraction of OC:

$$F_{OC}(T) = \frac{F_{Fh-OC} - F_{Fh}(0)F_{Fh}(T)}{1 - F_{Fh}(0)} \quad (2)$$

$$F_{Fh}(0) = 1 - \frac{TOC}{F_C} \quad (3)$$

where $F_{OC}(T)$ is the residual fraction of OC at a certain temperature, $F_{Fh\text{-}OC}$ is the residual fraction of Fh-OC at a certain temperature (directly measured mass), $F_{Fh}(0)$ is the original mass fraction of Fh in Fh-OC co-precipitates,

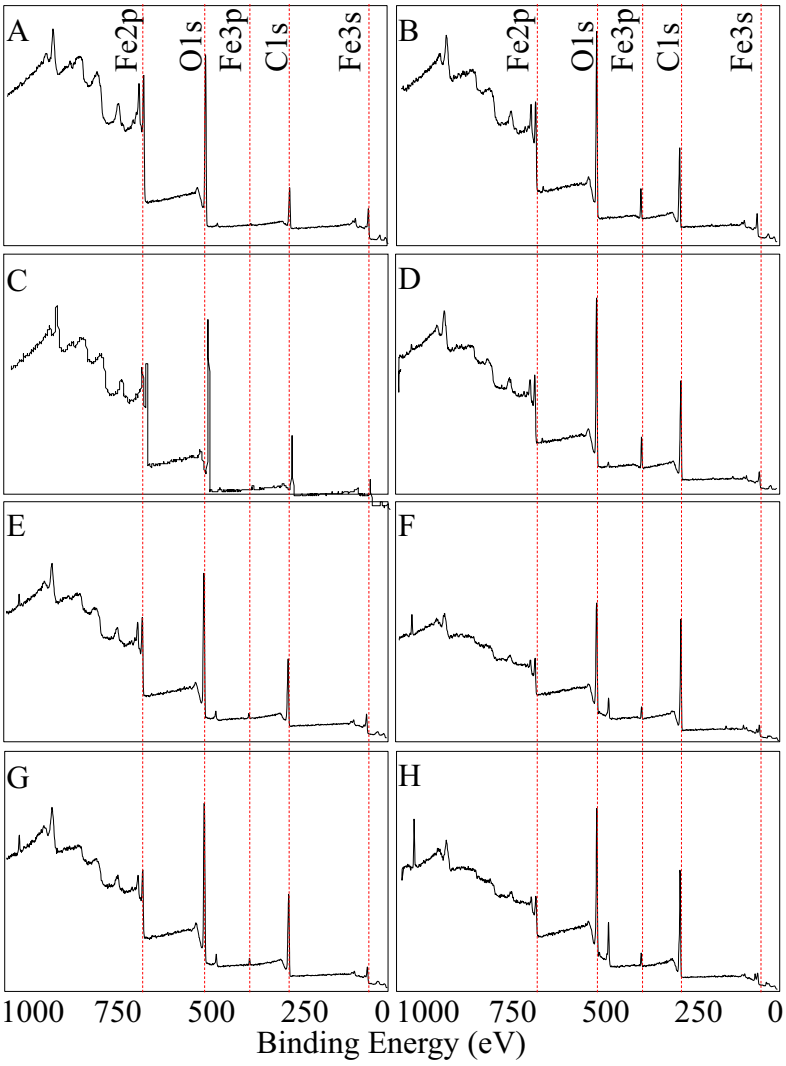

Fig. 5. Wide-range XPS analysis for Fh-OC co-precipitates before and after 288-h reduction. A, C, E, and G are for co-precipitates with C/Fe ratio of 0.7, 0.9, 1.8 and 3.7 before reduction, and B, D, F, H are for those corresponding co-precipitates after 288-h reduction, respectively.

$F_{Fh}(T)$ is the residual fraction of Fh at a certain temperature (directly measured for pure Fh), *TOC* is the original mass fraction of OC in Fh-OC (directly measured by an elemental analyzer, and *Fc* is the fraction of elemental C in the humic acid materials (0.60 IHSS, http://www.humicsubstances.org/). We assume the thermal stability of Fh in Fh-OC co-precipitate was same as for pure Fh. For Fh-OC with C/Fe ratio of 0.7, the $F_{OC}(T)$ decreased to 0 at 560 °C, when the corresponding temperature was 762 °C for Fh-OC with C/Fe ratio of 3.7 (Supplementary Data, Fig. S18). After the reduction, it is challenging to accurately calculate the $F_{OC}(T)$ because of various mineral transformations as shown by EXAFS. We used Eq. (2) to calculate the $F_{OC}(T)$ for only Fh-OC with C/Fe ratio of 1.8 and 3.7 after reduction, as the mineral transformation was smaller compared to Fh-OC with lower C/Fe ratios. The highest $F_{OC}(T)$ was 119% at 234 °C, because of the underestimate of the thermal stability of secondary minerals using the data collected for Fh. The final $F_{OC}(T)$ for Fh-OC with C/Fe ratio of 3.7 was 43.5%, much higher than that for original Fh-OC. The trend is similar for the Fh-OC with C/Fe ratio of 1.8.

4.3.4. Change in OC lability

Finally, we measured desorption of the Fh-bound OC as an indicator for the lability of OC. For co-precipitates with C/Fe ratio of 0.7, 0.9, 1.8 and 3.7, 7.3 ± 5.1, 5.0 ± 0.2, 5.3 ± 1.4 and 9.8 ± 0.2% of Fh-bound OC was desorbed after 4 days (Supplementary Data, Fig. S19). After reduction, 0–30.3% of Fh-bound OC was released to solution phase. Only Fh-OC with C/Fe ratio of 3.7 showed substantial desorption with a maximum level of releasable OC, which was enhanced by the reduction.

5. DISCUSSION

5.1. Fe reduction and mineral phase transformation

OC affects the reduction of Fe and mineral phase transformation through multiple ways. First, OC can enhance

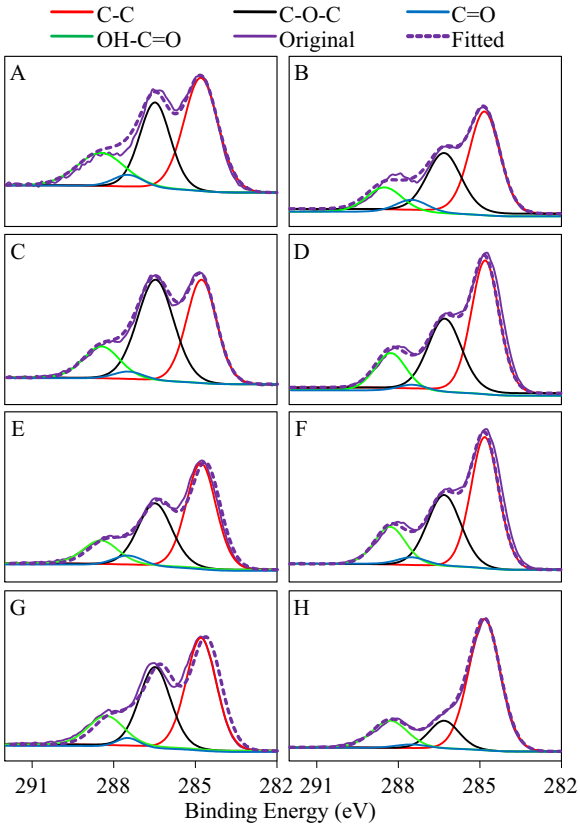

Fig. 6. Carbon 1s XPS spectra for Fh-OC co-precipitates before and after 288-h reduction. A, C, E, and G are for original Fh-OC co-precipitates with C/Fe ratio of 0.7, 0.9, 1.8 and 3.7, respectively. B, D, F and H are for Fh-OC co-precipitates after 288-h reduction.

the Fe reduction by accelerating extracellular electron transport (Kappler et al., 2004; Bose et al., 2009; Roden et al., 2010). Like in a previous study (Shimizu et al., 2013) there was a threshold value of C/Fe ratio between 1.8 and 3.7 to stimulate the reduction of Fe(III). Our additional experiments using higher C/Fe ratios of 4 and 4.9 showed more rapid reduction of Fe (Supplementary Data, Fig. S20). Jiang and Kappler (2008) demonstrated that minimal concentration of 5–10 mg C/L humic substances for stimulating extracellular electron transport. We also measured the HA-mediated electron transfer and electron accepting capacity (EAC) of HA and it was 2.43 mmol e^-/-mol C (Supplementary Data, Fig. S21). There can be differences in the EAC between dissolved and solid-phase OC. Roden et al. (2010) suggests that the EAC of solid-state OC could be 1/10 of that for dissolved OC. Using that factor, the EAC of Fh-bound OC would be 0.283 mmol e^-/-mol C. This will lead to a threshold EAC of Fe-bound OC to be 0.5–1.0 mmol e^-/mol Fe for facilitating the reduction of Fe. In addition, OC can also affect the Fe reduction through altering the particle size of precipitates and their dispersion. The average particle size for Fh-OC co-precipitates with C/Fe ratio of 0.7, 0.9, 1.8, and 3.7 was 1862, 2362, 1833, and 170 nm respectively, compared to 92 nm for Fh. As shown in previous studies (Mikutta, 2011; Amstaetter et al., 2012), OC can affect the particle size and aggregation of Fh by increasing repulsion between particles or acting as bridging materials. In systems with high C/Fe ratio, the sorption of OC on Fh surface can result in a net negative surface charge, which can minimize further aggregation of the co-precipitate particles due to electrostatic repulsion. However, in systems with lower C/Fe ratio, OC can act as a bridge to form larger aggregates. The relatively small size of co-precipitate with C/Fe ratio of 3.7 could facilitate its dispersion and Fe reduction.

Second, OC can protect Fh from reaction with Fe(II) and consequent mineral transformation, and increase the Fe reduction. Both aqueous and sorbed Fe(II) can promote the abiotic transformation of Fh to secondary minerals (Tronc et al., 1992; Yee et al., 2006; Liu et al., 2007). The transformation of Fh to more crystalline forms like goethite requires reconstructive transformation for poorly ordered octahedral units of Fh to edge-sharing octahedral units, which can be catalyzed by the presence of Fe(II) (Yee et al., 2006; Liu et al., 2007). The transformation of Fh to hematite is favored in the absence of Fe(II) via the process of dehydration and dehydroxylation (Yee et al., 2006). Electron exchange between Fe(II) and Fe(III) in Fh can

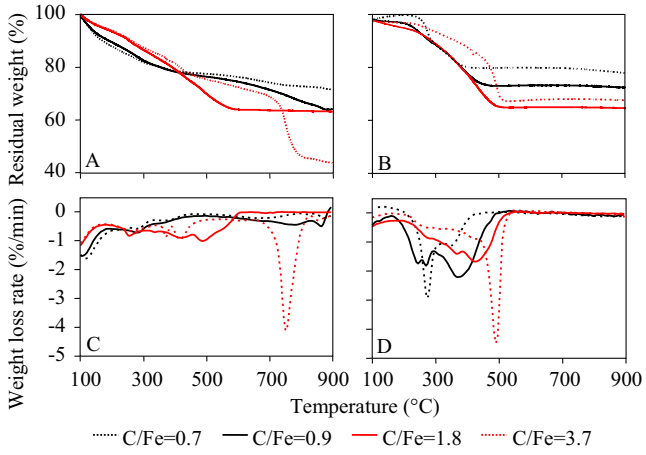

Fig. 7. Thermal gravimetric analysis (TGA) results for Fh-OC co-precipitates with C/Fe ratios ranging 0.7–3.7 before and after 288-h reduction: original temperature-dependent residual weight percentage (A and B); temperature-dependent weight loss rate (C and D).

enhance the reductive dissolution and mineral transformation of Fh (Chen et al., 2015). However, the presence of DOC can inhibit the interactions of Fe(II) and Fh by chelating with Fe(II). Strong complexation between DOC and Fe(II) can also reduce the rate of electron transfer between Fe(II) and Fe(III) as well as dissolution and recrystallization of Fh. In addition, at higher C/Fe ratio, OC in the complex can act as a physical barrier to prevent interactions between Fe(II) and Fh by blocking the surface sites (Chen et al., 2015). In addition to impacting the extent of secondary mineral formation, the mineral transformation pathway was also altered by the presence of OC. Increasing C/Fe ratio favored magnetite formation and retarded lepidocrocite. For example, for co-precipitates with C/Fe ratio of 0.7, 0.9, 1.8 and 3.7, percent of lepidocrocite were 34.7%, 21.7%, 8.5%, and 0%, and percent of magnetite were 0%, 15.2%, 22.5%, and 21.5%, respectively (Supplementary Data, Table S6). The presence of OC increased the formation of goethite, although further increase of C/Fe ratio decreased the formation of goethite (Supplementary Data, Table S6). Goethite and lepidocrocite are formed through Ostwald ripening of Fh, and OC could prevent the further transformation of lepidocrocite to goethite (Cornell and Schwertmann, 1996; Shimizu et al., 2013; Chen et al., 2015). The Fh-OC co-precipitate with C/Fe of 3.7 showed increased percent of Fe(II) in solution phase (Supplementary Data, Fig. S3); at 288 h, 39.5% of Fe(II) was in solution, as compared to 4.7% of Fe(II) in solution for pure Fh respectively. Formation of multiple types of secondary Fe minerals implies that the Fe mineral phase transformation was regulated by interactions between Fe(II), OC, and Fh.

Third, OC covering on the surface and complexing with Fh can inhibit the accessibility of Fe to microbial reduction (Amstaetter et al., 2012; Shimizu et al., 2013). Especially, inner-sphere coordination between OC and Fe oxide prevents Fh from microbial reduction (Brunschwig et al., 1982; Johnson et al., 1998). Potential blockage of Fh surface reaction sites by OC can also inhibit the microbial reduction (Shimizu et al., 2013; Chen et al., 2015). Furthermore, decrease in surface area corresponding to increase in C/Fe could reduce the number of surface sites for interactions between bacteria and co-precipitates. Decreased Fe reduction rate for co-precipitates with lower C/Fe ratio was likely due to both reduced surface area and increased site blockage by OC. However, for co-precipitates with C/Fe ratio of 3.7, the electron shuttling by OC played a greater role in regulating the Fe reduction than surface area and site blockage due to OC. The overall impact of associated OC on Fe reduction would be a result of combined effects.

5.2. OC release and transformation during reduction

Our previous studies showed that hematite-bound OC was released at a much faster rate than Fe reduction during the initial stage of reduction (Adhikari and Yang, 2015; Adhikari et al., 2016). Compared to hematite, Fh has higher surface area as well as a higher capacity for incorporation and sorption of OC, yet it can be reduced more easily and rapidly than hematite (Bose et al., 2009; Xu et al., 2016). Therefore, the dynamics of OC release during microbial reduction are likely to be complex, as our results show, the C/Fe ratio clearly playing an important role in the processes.

For co-precipitates with C/Fe ratio of 3.7, there were strong correlations (Pearson correlation coefficient $r = 0.97$, significance $p = 0.01$) between the percentage of DOC release (as compared to total OC content) and Fe reduction (as compared to total Fe in the Fh-OC co-precipitate) (Supplementary Data, Fig. S22; Table S11). Similar correlations were also observed between the concentrations of DOC and concentration of dissolved, solid-associated, and total Fe(II) ($r = 0.97$, $p = 0.01$). These correlations indicate that the reduction and dissolution of Fh was a governing process for the release of DOC, consistent with a recently published study (Pan et al., 2016).

The $SUVA_{254}$ for the released OC was much lower compared to that of the original HA ($SUVA_{254} = 8.7$) (Fig. 4). For the synthesis of Fh-OC co-precipitates, the $SUVA_{254}$ for OC in supernatant after centrifugation of Fh-OC was 7.4, indicating aromatic OC was preferentially co-precipitated with Fh. Such comparison indicates that the aromatic fraction of the original OC was preferentially retained in the Fh-OC co-precipitates during the reduction process. Carbon NEXAFS spectroscopy data also showed an increased fraction of phenolic carbon in the residual fraction of the co-precipitates after reduction (Supporting Data, Fig. S23). This is different from the observations for hematite-OC sorption complex, for which aromatic OC was more easily released during the reduction reaction (Adhikari and Yang, 2015; Adhikari et al., 2016). Our result is consistent with previous findings that phenolic and oxalic ligands stabilized Fe(III) and consequent Fe-OC co-precipitates (Varela and Tien, 2003; Hall and Silver, 2015).

In our system, OC was not used as an electron donor for Fe reduction. Measurement of CO_2 in headspace indicated minimal oxidation of OC (<0.01%) during the anaerobic reduction of Fh (Fig. 8). These results are consistent with the well-known inability of Shewanella and other dissimilatory Fe(III)-reducing bacteria to degrade complex organic carbon compounds coupled to Fe(III) reduction (Lovley, 2000). There was no substantial generation of CH_4 either. All these results suggest the transformation of Fh-bound OC was mainly occurring in aqueous phase. On the surface of Fh-OC co-precipitates, the relative fraction of COOH vs. C—O—C increased after the reduction (Fig. 6). This indicates the COOH was more resistant to reductive release, likely as a result of ligand complexation with Fe. The relative increase was greatest for Fh-OC co-precipitates with a C/Fe ratio of 3.7, for which the reductive release was much higher than other co-precipitates. Reduction led to the change in structure of Fh-OC co-precipitates, and shift in the surface chemistry of Fh-bound OC. Together with $SUVA_{254}$ analysis, our results indicate that aromatic/carboxylic-enriched OC was selectively retained in the solid-phase during the reduction of Fh.

Selective retention of aromatic/carboxylic-enriched OC was also supported by the thermal analysis. Based on the

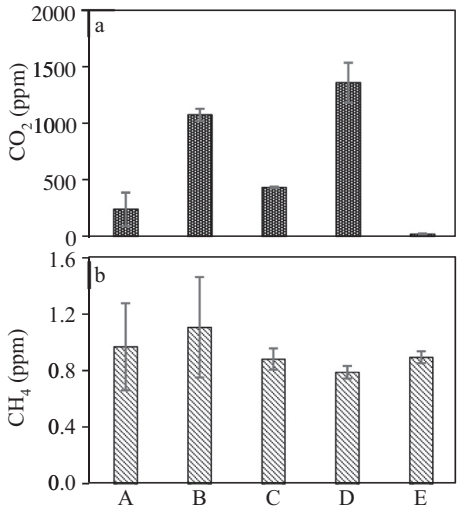

Fig. 8. Measure of CO_2 (a) and CH_4 (b) concentration in the headspace after 12-day incubation. Error bars indicate standard deviations ($n = 3$). Several systems and controls have been measured: (A) blank for glove box only; (B) strain CN32 only; (C) strain CN32 with Fh; (D) strain CN32 with OC (only dissolved HA, 48 mM C); (E) strain CN32 with Fh-OC co-precipitate with C/Fe ratio of 3.7, (13 mM Fe). Other experimental conditions were same as those in the microbial reduction. For the system with strain CN32 and Fh-OC co-precipitate (C/Fe = 3.7), CO_2 and CH_4 accounted for 5.1×10^{-3}% and 2.4×10^{-4}% of the total carbon added as co-precipitates.

calculated F_{OCT}, thermal stability of Fe-bound OC increased with the C/Fe ratio (Fig. 7; Supplementary Data, Fig. S18). Association with Fe can likely increase the thermal stability of OC by complexation between Fe oxides and OC and increase in the related bond strength. After the reduction, the thermal stability of Fe-bound OC was increased for Fh-OC co-precipitates with C/Fe of 1.8 and 3.7, and this was likely caused by the preferential retention of Fh-OC co-precipitates. Johnson et al. (2015) observed that sorption to manganese (Mn) oxide increased the thermal stability of OC, as a result of inner-sphere binding between OC and Mn oxides. These findings are consistent with the increase in the percent of carboxylic functional groups after reduction, as shown by XPS.

5.3. Lability of residual OC

For Fh-OC with C/Fe ratio of 3.7, we fit the kinetics for DOC with the equation:

$$F_{DOC} = F_{DOC_0} + F_{DOCs}(1 - \exp(-kt)) \quad (4)$$

where F_{DOC} is the time-dependent fraction of DOC versus total OC in the complex, F_{DOC0} is the fraction of original DOC versus TOC, F_{DOCs} is the steady-level reductive release fraction of DOC versus total OC in the co-precipitate, k (h^{-1}) is the first order rate constant for the desorption, and t is time (h). For Fh-OC co-precipitate with C/Fe ratio of 3.7, both the F_{DOCs} and k were significantly increased upon the reduction, from 7.4% and 0.02 h^{-1} to 17.3% and 0.04 h^{-1}. This indicates, along with the reduction release of Fh-bound OC, the lability of OC was also increased partially due to the enrichment of C on the surface shown in XPS analysis.

XPS results showed a substantial increase in C/Fe ratio after the reduction compared to original Fh-OC co-precipitates. The contribution to surface C/Fe ratio from bacteria biomass was low, as observed in pure Fh reacted with strain CN32. After 288 h of reduction, the C/Fe ratio on the surface of pure Fh increased from 1.3 to 5.2. This indicated that the major influence on surface enrichment of C was caused by the alteration in Fh-OC co-precipitates rather than from biomass. It is possible that surface Fe(III) weakly complexed with OC was readily reduced, which could increase surface C/Fe ratio. The increased surface C/Fe ratio can also be contributed by the sorption of released DOC on the residual Fh-OC, through both Fe-OC interactions and OC-OC interactions (Hedges and Keil, 1995). The higher content of OC on the surface after reduction can lead to the higher mobility of OC, as shown for the Fh-OC co-precipitates with a C/Fe ratio of 3.7.

Overall, our results provided comprehensive analysis for the dynamics of Fh-OC co-precipitates in the microbial reduction. Compared to a previous similar study performed by Shimizu et al. (2013), there are critical differences. This study is focused more on the release and transformation of OC, when Shimizu et al. (2013) emphasized the impact of co-precipitated OC on the Fe reduction and mineral transformation. We have measured the electron shutting capacity of HA directly in this study, and used it to interpret the role of HA in the redox reactions. In addition, we have used multiple analysis, including XPS, UV analysis, C1s NEXAFS, and CO_2/CH_4 measurement, to determine the release and transformation of OC. The desorption in DI water for the Fe-bound OC was measured as an indicator for the mobility of OC. Last not least, we directly used co-precipitates, when the previous study used the precipitate-coated sands.

6. CONCLUSIONS

Our results demonstrated that the reduction of Fh-OC co-precipitates by facultative Fe-reducing bacteria (CN32) can release a significant amount of OC, depending on the initial solid-phase C/Fe ratio. For Fh-OC co-precipitates with C/Fe ratio of 3.7, 54.7% of Fh-bound OC was released, when 25.1% of Fe was reduced. Release of Fh-bound OC was not observed for co-precipitates with C/Fe ratio of 0.7, 0.9, and 1.8. The residual OC in co-precipitate with C/Fe ratio of 3.7 after reduction was more easily desorbed compared to original Fh-bound OC, and potentially more available for microbial degradation (Keil et al., 1994; Kalbitz et al., 2005). After the reduction, Fh-bound OC was more concentrated on the surface of co-precipitates, enriched in the carboxylic functional group on the surface, and the aromatic in the bulk. Surface enrichment will likely make the Fh-bound OC more accessible for microbial degradation, even without release to the solution phase. Our findings highlight that reductive release and transformation will be important for the degradation of

Fh-bound OC, especially under the scheme of dynamic climate with more extreme precipitation events and changing water cycles.

In this study, we used a pure culture of strain CN32, which reduced Fe(III) but did not degrade/mineralize OC. Using strain CN32 provided an opportunity to study the release of Fh-bound OC and transformation of structure of Fh-OC co-precipitates, but not the degradation or mineralization of OC. It deserves further efforts to analyze the degradation and mineralization of Fe-bound OC during reduction by a natural microbial community, which contains both Fe reducer and OC degrader. Finally, it must be noted that the results obtained with the model HA may not translate directly to the behavior of natural organic matter in soils and sediments, e.g. due to the differences in the chemical composition of HA and natural organic matter (Schmidt et al., 2011; Lehmann and Kleber, 2015). However, extensive studies showed the electron shuttling capacity of HA, which can serve as a good model of redox-active natural OC (Lovley, 2000; Jiang and Kappler, 2008; Roden et al., 2010). Our on-going studies of behavior of natural OC during the Fe reduction process will provide valuable comparison between natural OC and the model HA.

ACKNOWLEDGEMENT

This research was supported by University of Nevada-Reno Startup fund, DOE grant DE-SC0014275 and USDA grant 2015-67018-23120. YT and RH acknowledge funding support from Georgia Institute of Technology and American Chemical Society Petroleum Research Fund (#54143-DNI5). We acknowledge that the DLS measurements were performed by Pushpa Chhetri and Ganesh R. Rana at the Department of Chemistry, UNR under the supervision of M. Alpuche-Aviles. We thank Suzyanne Guzicki and Dr. Jeremy Fein at University of Notre Dame for help with discussion about surface area. The DLS was acquired with funds from NSF CAREER Award No. CHE-1255387 for MAA. The support of the National Science Foundation (CHE-1429768) for the purchase of the powder X-ray diffractometer is gratefully acknowledged. We thank Elizabeth Tomaszewski from University of Wisconsin-Madison for help with performing NEXAFS analysis at CLS. We also thank Dr. Sarrah M. Dunham-Cheatham at University of Nevada-Reno for help with editing the manuscript.

APPENDIX A. SUPPLEMENTARY MATERIAL

Supplementary data associated with this article can be found, in the online version, at http://dx.doi.org/10.1016/j.gca.2017.06.017.

REFERENCES

Adhikari D., Poulson S. R., Sumaila S., Dynes J. J., McBeth J. M. and Yang Y. (2016) Asynchronous reductive release of iron and organic carbon from hematite-humic acid complexes. *Chem. Geol.* **430**, 13–20.

Adhikari D. and Yang Y. (2015) Selective stabilization of aliphatic organic carbon by iron oxide. *Sci. Rep.* **5**, 11214.

Amstaetter K., Borch T. and Kappler A. (2012) Influence of humic acid imposed changes of ferrihydrite aggregation on microbial Fe(III) reduction. *Geochim. Cosmochim. Acta* **85**, 326–341.

Appelo C. A. J., Van der Weiden M. J. J., Tournassat C. and Charlet L. (2002) Surface complexation of ferrous iron and carbonate on ferrihydrite and the mobilization of arsenic. *Environ. Sci. Technol.* **36**, 3096–3103.

Biesinger M. C., Payne B. P., Grosvenor A. P., Lau L. W. M., Gerson A. R. and Smart R. S. (2011) Resolving surface chemical states in XPS analysis of first row transition metals, oxides and hydroxides: Cr, Mn, Fe, Co and Ni. *Appl. Surf. Sci.* **257**, 2717–2730.

Bose S., Hochella M. F., Gorby Y. A., Kennedy D. W., McCready D. E., Madden A. S. and Lower B. H. (2009) Bioreduction of hematite nanoparticles by the dissimilatory iron reducing bacterium *Shewanella oneidensis* MR-1. *Geochim. Cosmochim. Acta* **73**, 962–976.

Brunschwig B. S., Creutz C., Macartney D. H., Sham T. K. and Sutin N. (1982) The role of inner-sphere configuration changes in electron-exchange reactions of metal complexes. *Faraday Discuss. Chem. Soc.* **74**, 113–127.

Chacon N., Silver W. L., Dubinsky E. A. and Cusack D. F. (2006) Iron reduction and soil phosphorus solubilization in humid tropical forests soils: the roles of labile carbon pools and an electron shuttle compound. *Biogeochemistry* **78**, 67–84.

Chen C. M., Dynes J. J., Wang J. and Sparks D. L. (2014) Properties of Fe-organic matter associations via coprecipitation versus adsorption. *Environ. Sci. Technol.* **48**, 13751–13759.

Chen C. M., Kukkadapu R. and Sparks D. L. (2015) Influence of coprecipitated organic matter on Fe-(aq)(2+)-catalyzed transformation of ferrihydrite: implications for carbon dynamics. *Environ. Sci. Technol.* **49**, 10927–10936.

Cheng C. H., Lehmann J., Thies J. E., Burton S. D. and Engelhard M. H. (2006) Oxidation of black carbon by biotic and abiotic processes. *Org. Geochem.* **37**, 1477–1488.

Cornell R. M. and Schwertmann U. (1996) *The Iron Oxides: Structure, Properties, Reactions, Occurrences and Uses*. Federal Republic of Germany.

Dufrene Y. F., VanderWal A., Norde W. and Rouxhet P. G. (1997) X-ray photoelectron spectroscopy analysis of whole cells and isolated cell walls of gram-positive bacteria: comparison with biochemical analysis. *J. Bacteriol.* **179**, 1023–1028.

Elsner M., Schwarzenbach R. P. and Haderlein S. B. (2004) Reactivity of Fe(II)-bearing minerals toward reductive transformation of organic contaminants. *Environ. Sci. Technol.* **38**, 799–807.

Eusterhues K., Hadrich A., Neidhardt K., Kusel K., Keller T. F., Jandt K. D. and Totsche K. U. (2014b) Reduction of ferrihydrite with adsorbed and coprecipitated organic matter: microbial reduction by Geobacter bremensis vs. abiotic reduction by Na-dithionite. *Biogeosciences* **11**, 4953–4966.

Eusterhues K., Neidhardt J., Haedrich A., Kuesel K. and Totsche K. U. (2014a) Biodegradation of ferrihydrite-associated organic matter. *Biogeochemistry* **119**, 45–50.

Fredrickson J. K., Zachara J. M., Kennedy D. W., Dong H. L., Onstott T. C., Hinman N. W. and Li S. M. (1998) Biogenic iron mineralization accompanying the dissimilatory reduction of hydrous ferric oxide by a groundwater bacterium. *Geochim. Cosmochim. Acta* **62**, 3239–3257.

Grosvenor A. P., Kobe B. A., Biesinger M. C. and McIntyre N. S. (2004) Investigation of multiplet splitting of Fe 2p XPS spectra and bonding in iron compounds. *Surf. Interface Anal.* **36**, 1564–1574.

Gu B. H., Schmitt J., Chen Z., Liang L. Y. and McCarthy J. F. (1995) Adsorption and desorption of different organic-matter fractions on iron-oxide. *Geochim. Cosmochim. Acta* **59**, 219–229.

Hall S. J. and Silver W. L. (2015) Reducing conditions reactive metals and their interactions can explain spatial patterns of

surface soil carbon in a humid tropical forest. *Biogeochemistry* **125**, 149–165.

Hansel C. M., Benner S. G., Neiss J., Dohnalkova A., Kukkadapu R. K. and Fendorf S. (2003) Secondary mineralization pathways induced by dissimilatory iron reduction of ferrihydrite under advective flow. *Geochim. Cosmochim. Acta* **67**, 2977–2992.

Hansel C. M., Benner S. G., Nico P. and Fendorf S. (2004) Structural constraints of ferric (hydr)oxides on dissimilatory iron reduction and the fate of Fe(II). *Geochim. Cosmochim. Acta* **68**, 3217–3229.

Hedges J. I. and Keil R. G. (1995) Sedimentary organic matter preservation: an assessment and speculative synthesis. *Mar. Chem.* **49**, 81–115.

Jambor J. L. and Dutrizac J. E. (1998) Occurrence and constitution of natural and synthetic ferrihydrite a widespread iron oxyhydroxide. *Chem. Rev.* **98**, 2549–2585.

Jiang J. and Kappler A. (2008) Kinetics of microbial and chemical reduction of humic substances: implications for electron shuttling. *Environ. Sci. Technol.* **42**, 3563–3569.

Johnson T. L., Fish W., Gorby Y. A. and Tratnyek P. G. (1998) Degradation of carbon tetrachloride by iron metal: complexation effects on the oxide surface. *J. Contam. Hydrol.* **29**, 379–398.

Johnson K., Purvis G., Lopez-Capel E., Peacock C., Gray N., Wagner T., März C., Bowen L., Ojeda J., Finlay N. and Robertson S. (2015) Towards a mechanistic understanding of carbon stabilization in manganese oxides. *Nat. Commun.* **6**.

Kaiser K. and Guggenberger G. (2007) Sorptive stabilization of organic matter by microporous goethite: sorption into small pores vs. surface complexation. *Eur. J. Soil Sci.* **58**, 45–59.

Kalbitz K., Schwesig D., Rethemeyer J. and Matzner E. (2005) Stabilization of dissolved organic matter by sorption to the mineral soil. *Soil Biol. Biochem.* **37**, 1319–1331.

Kappler A., Benz M., Schink B. and Brune A. (2004) Electron shuttling via humic acids in microbial iron(III) reduction in a freshwater sediment. *FEMS Microbiol. Ecol.* **47**, 85–92.

Keil R. G., Hu F. S., Tsamakis E. C. and Hedges J. I. (1994) Pollen in marine-sediments as an indicator of oxidation of organic-matter. *Nature* **369**, 639–641.

Kukkadapu R. K., Zachara J. M., Fredrickson J. K., Smith S. C., Dohnalkova A. C. and Russell C. K. (2003) Transformation of 2-line ferrihydrite to 6-line ferrihydrite under oxic and anoxic conditions. *Am. Mineral.* **88**, 1903–1914.

Lalonde K., Mucci A., Ouellet A. and Gelinas Y. (2012) Preservation of organic matter in sediments promoted by iron. *Nature* **483**, 198–200.

Lehmann J., Solomon D., Brandes J., Fleckenstein H., Jacobson C. and Thieme J. (2009) Synchrotron-based near-edge X-ray spectroscopy of natural organic matter in soils and sediments. *Biophysico-Chemical Processes Involving Natural Nonliving Organic Matter in Environmental Systems*, pp. 729–781.

Lehmann J. and Kleber M. (2015) The contentious nature of soil organic matter. *Nature* **528**, 60–68.

Liu H., Li P., Zhu M. Y., Wei Y. and Sun Y. H. (2007) Fe(II)-induced transformation from ferrihydrite to lepidocrocite and goethite. *J. Solid State Chem.* **180**, 2121–2128.

Lovley D. R. (2000) *Fe(III) and Mn(IV) Reduction. Environmental Microbe-Metal Interactions*. ASM Press, Washington, DC, pp. 3–30.

McIntyre N. S. and Zetaruk D. G. (1977) X-ray photoelectron spectroscopic studies of iron-oxides. *Anal. Chem.* **49**, 1521–1529.

Mikutta C. (2011) X-ray absorption spectroscopy study on the effect of hydroxybenzoic acids on the formation and structure of ferrihydrite. *Geochim. Cosmochim. Acta* **75**, 5122–5139.

Neal A. L., Lowe K., Daulton T. L., Jones-Meehan J. and Little B. J. (2002) Oxidation state of chromium associated with cell surfaces of *Shewanella oneidensis* during chromate reduction. *Appl. Surf. Sci.* **202**, 150–159.

Newville M. (2001) IFEFFIT: interactive XAFS analysis and FEFF fitting. *J. Synchrotron Radiat.* **8**, 322–324.

Nguyen B. T., Lehmann J., Kinyangi J., Smernik R., Riha S. J. and Engelhard M. H. (2008) Long-term black carbon dynamics in cultivated soil. *Biogeochemistry* **89**, 295–308.

Ojeda J. J., Romero-Gonzalez M. E., Bachmann R. T., Edyvean R. G. J. and Banwart S. A. (2008) Characterization of the cell surface and cell wall chemistry of drinking water bacteria by combining XPS FTIR spectroscopy modeling and potentiometric titrations. *Langmuir* **24**, 4032–4040.

Pan W., Kan J., Inamdar S., Chen C. and Sparks D. (2016) Dissimilatory microbial iron reduction release DOC (dissolved organic carbon) from carbon-ferrihydrite association. *Soil Biol. Biochem.* **103**, 232–240.

Roden E. E. (2004) Analysis of long-term bacterial vs. chemical Fe (III) oxide reduction kinetics. *Geochim. Cosmochim. Acta* **68**, 3205–3216.

Roden E. E. (2003) Fe(III) oxide reactivity toward biological versus chemical reduction. *Environ. Sci. Technol.* **37**, 1319–1324.

Roden E. E. (2006) Geochemical and microbiological controls on dissimilatory iron reduction. *C. R. Geosci.* **338**, 456–467.

Roden E. E., Kappler A., Bauer I., Jiang J., Paul A., Stoesser R., Konishi H. and Xu H. (2010) Extracellular electron transfer through microbial reduction of solid-phase humic substances. *Nat. Geosci.* **3**, 417–421.

Schmidt M. W. I., Torn M. S., Abiven S., Dittmar T., Guggenberger G., Janssens I. A., Kleber M., Kogel-Knabner I., Lehmann J., Manning D. A. C., Nannipieri P., Rasse D. P., Weiner S. and Trumbore S. E. (2011) Persistence of soil organic matter as an ecosystem property. *Nature* **478**, 49–56.

Shimizu M., Zhou J., Schroeder C., Obst M., Kappler A. and Borch T. (2013) Dissimilatory reduction and transformation of ferrihydrite-humic acid coprecipitates. *Environ. Sci. Technol.* **47**, 13375–13384.

Stookey L. L. (1970) Ferrozine - a new spectrophotometric reagent for iron. *Anal. Chem.* **42**, 779–781.

Tipping E. (1981) The adsorption of aquatic humic substances by iron-oxides. *Geochim. Cosmochim. Acta* **45**, 191–219.

Tronc E., Belleville P., Jolivet J. P. and Livage J. (1992) Transformation of ferric hydroxide into spinel by iron (II) adsorption. *Langmuir* **8**, 313–319.

Varela E. and Tien M. (2003) Effect of pH and oxalate on hydroquinone-derived hydroxyl radical formation during brown rot wood degradation. *Appl. Environ. Microbiol.* **69**, 6025–6031.

Wagai R. and Mayer L. M. (2007) Sorptive stabilization of organic matter in soils by hydrous iron oxides. *Geochim. Cosmochim. Acta* **71**, 25–35.

Webb S. M. (2005) SIXpack: a graphical user interface for XAS analysis using IFEFFIT. *Phys. Scripta* **2005**, 1011–1014.

Weber K. A., Urrutia M. M., Churchill P. F., Kukkadapu R. K. and Roden E. E. (2006) Anaerobic redox cycling of iron by freshwater sediment microorganisms. *Appl. Environ. Microbiol.* **8**, 100–113.

Weishaar J. L., Aiken G. R., Bergamaschi B. A., Fram M. S., Fujii R. and Mopper K. (2003) Evaluation of specific ultraviolet absorbance as an indicator of the chemical composition and reactivity of dissolved organic carbon. *Environ. Sci. Technol.* **37**, 4702–4708.

Xu S. N., Adhikari D., Huang R. X., Zhang H., Tang Y. Z., Roden E. and Yang Y. (2016) Biochar-facilitated microbial reduction of hematite. *Environ. Sci. Technol.* **50**, 2389–2395.

Yang Y., Saiers J. E., Xu N., Minasian S. G., Kozimor S. A., Tyliszczak T., Shuh D. K. and Barnett M. O. (2012) Impact of natural organic matter on uranium transport through saturated geologic materials: from molecular to column scale. *Environ. Sci. Technol.* **46**, 5931–5938.

Yang Y., Shu L., Wang X. L., Xing B. S. and Tao S. (2011) Impact of de-ashing humic acid and humin on organic matter structural properties and sorption mechanisms of phenanthrene. *Environ. Sci. Technol.* **45**, 3996–4002.

Yee N., Shaw S., Benning L. G. and Nguyen T. H. (2006) The rate of ferrihydrite transformation to goethite via the Fe(II) pathway. *Am. Mineral.* **91**, 92–96.

Zachara J. M., Ainsworth C. C., Cowan C. E. and Thomas B. L. (1987) Sorption of binary-mixtures of aromatic nitrogen heterocyclic-compounds on subsurface materials. *Environ. Sci. Technol.* **21**, 397–402.

Zhao Q., Poulson S. R., Obrist D., Sumaila S., Dynes J. J., McBeth J. M. and Yang Y. (2016) Iron-bound organic carbon in forest soils: quantification and characterization. *Biogeosciences* **13**, 4777–4788.

Zhao Q., Adhikari D., Huang R., Patel A., Wang X., Tang Y., Obrist D., Roden E. E. and Yang Y. (2017) Coupled dynamics of iron and iron-bound organic carbon in forest soils during anaerobic reduction. *Chem. Geol.* **464**, 118–126.

Associate editor: Marc Norman